The Jahn-Teller effect in icosahedral symmetry: ground-state topography and phases

1994 J. Phys.: Condens. Matter 6 9017

(http://iopscience.iop.org/0953-8984/6/43/008)

J. Phys.: Condens. Matter 6 (1994) 9017–9041. Printed in the UK

The Jahn–Teller effect in icosahedral symmetry: ground-state topography and phases

J P Cullerne and M C M O'Brien

Oxford University Department of Physics, Theoretical Physics, 1 Keble Road, Oxford OX1 3NP, UK

Received 9 March 1994, in final form 29 July 1994

Abstract. The resurgence of interest in properties of molecules of icosahedral symmetry follows the discovery of the C_{60} molecule. Because of the high symmetry almost all the electronic and vibrational states are highly degenerate, so in dealing with properties of these systems their Jahn–Teller interactions must almost always be allowed for. In this paper we explore the ground states of the $G \otimes (g \oplus h)$ coupling scheme and those of the two subsystems, $G \otimes g$ and $G \otimes h$. Using a mixture of analytical and numerical methods, we map the lowest adiabatic potential energy surfaces of these systems. The mappings are made in such a way as to facilitate an analysis of the geometrical phase factor acquired by the quantal system on transportation round adiabatic circuits in parameter space. These geometrical phase factors, or Berry phases, depend greatly on the paths followed to complete these circuits. In this paper we introduce parametrizations that elucidate with ease such circuits and lead to simple and easily accessible graphical illustrations of the subsequently induced Berry phases. Finally, we use the information provided by the Berry phase analysis to obtain the correct ordering of the low-lying states at strong coupling, the energies of these states and the Ham factors of the Jahn–Teller-active operators within these states.

1. Jahn–Teller interactions in the icosahedral group

Until the recent discovery of the C_{60} molecule [1], the icosahedral symmetry group did not figure largely in discussions of the Jahn–Teller effect. It was not thought until the last decade that molecules with this high symmetry would be found to exist. In fact the range of Jahn–Teller interactions within the different irreducible representations of this group is so rich and varied that they are well worth studying and classifying even before possible manifestations of some of them appear in the experimental record.

A useful paper giving much of what we need to know about the icosahedral group is one by Judd [2], which gives the character tables of both the single and double icosahedral groups, and the breakdown of angular momentum eigenstates into their irreducible representations. There are five irreducible representations in the single group: one singlet, A, two triplets, T_1 and T_2, one quartet, G, and one quintet, H. (The notation is rather variable in the literature, but this is what we shall use here.) Study of the products of representations shows that six Jahn–Teller couplings must be considered. Those involving only single modes are, listed in the form electronic state $\otimes$ vibrational state, $T_1 \otimes h$, $T_2 \otimes h$, $G \otimes g$, $G \otimes h$, $H \otimes g$ and $H \otimes h$. A survey of the continuous group invariances produced by involving several modes in these Jahn–Teller systems was made by Pooler [3]. The properties are listed below. For brevity, in all of the following we denote coupling schemes by just the symmetry designations with a subscript 'eq', for equal coupling.

0953-8984/94/439017+25$19.50

(i) T⊗h. The interaction matrices in these systems are exactly the same as those coupling a triplet simultaneously to ϵ- and τ_2-modes in cubic symmetry in the case where the two sets of modes combine together to act as a quintet of modes. This case, which occurs surprisingly often in cubic symmetry considering that it is an 'accidental' degeneracy, has been extensively studied. The Hamiltonian has rotational symmetry in a three-dimensional sub-space of the five-dimensional phase space, with the result that the low-lying states are rather closely spaced, being pseudo-rotational. This type of coupling is the important one for low-lying excited states of C_{60} because they are electronic triplets [4, 5, 6, 7, 8].

(ii) G⊗($g \oplus h$). Because the symmetric square of G contains both G and H, the general Jahn–Teller system includes coupling to modes of both these types. Pooler [3] shows that with the strengths of coupling to both types of mode suitably adjusted the Hamiltonian is invariant under SO(4), so there will be a continuum of minima. Ceulemans and Fowler [9] treated this coupling scheme, providing a general solution for the full G⊗($g \oplus h$) system.

(iii) G⊗g. Here the lowest APES has minima as well as threefold degeneracies at points corresponding to distortions of tetrahedral symetry, and saddle points and degeneracies at distortions of D_{3h} symmetry.

(iv) G⊗h. Here the lowest APES has ten points of minimum energy, corresponding to distortions of D_{3h} symmetry, saddle points are at distortions of D_{2h} symmetry, and degeneracies at distortions of D_{3h} symmetry. Minima lie at the vertices of a dodecahedron embedded in the five-dimensional phase space, while the saddle points nearest in energy to the minima lie near the centres of the edges of the dodecahedron.

(v) H⊗($g \oplus h \oplus h$). An extra complication is introduced here because the H irreducible representation occurs twice in the symmetrical product H⊗H. As a result the Wigner–Eckart theorem does not take its usual simple form, and there are two families of matrices that must be multiplied by different coupling constants to represent a general Jahn–Teller interaction. The two different types of h-matrices are often distinguished by deriving one from a set of $J = 2$ states (h_2) and one from a set of $J = 4$ states (h_4). Once again, the general solution for the full H⊗($g \oplus h \oplus h$) system was treated by Ceulemans et al [10]. Some of the possible variations may be listed (vi) to (ix) below.

(vi) H⊗($g \oplus h_2 \oplus h_4$). Pooler [3] shows that the Hamiltonian can have SO(5) symmetry if all three sets of modes are included with appropriate coupling constants.

(vii) H⊗($g \oplus h_4$). Here, again with appropriate coupling constants, the Hamiltonian can have SO(3) symmetry [3].

(viii) H⊗h_2. This is the case that was considered by Khlopin *et al* [11]. The symmetry is SO(3) [3]. The lowest APES is a four-dimensional hypersphere in the five-dimensional phase space, and it becomes degenerate with the next APES over a three-dimensional sub-space. This can be expected to lead to even higher degeneracies in the closely spaced low-lying levels than in T ⊗ h. We shall have to return to this system later.

(ix) H⊗g. This has no continuous group symmetry. The lowest APES has minima and degeneracies at points of D_{3h} distortion, and saddle points and degeneracies at distortions of tetrahedral symmetry.

We should mention here that any real cluster with this symmetry is almost bound to be large enough to have many different vibrations of each type; however, it is always possible to take a linear combination of the normal coordinates as an effective mode in such a way that coupling to this one mode is a best first approximation to the larger Hamiltonian [12, 11, 13]. This is why it makes sense to work in an approximation that uses only one mode of each symmetry, which we shall do in what follows.

2. General discussion and plan of the paper

The icosahedral orbital quartet G is Jahn–Teller active under the nine normal-mode distortions belonging to the icosahedral representation $(g \oplus h)$. The work of Ceulemans *et al* [9] provides an elegant general solution for the full system $G\otimes(g \oplus h)$ that had only previously been treated in part by Khlopin *et al* [11]. Ceulemans *et al* [9] appealed to the *epikernel principle* [14, 15] to obtain the extremal configurations and extensive use was made of the finite and infinite invariances present in the $G\otimes(g \oplus h)$ problem. In this vein, the symmetry of the system splits naturally into three categories: the symmetries of the infinite SO(4) parent group, the finite icosahedral group of the Jahn–Teller origin, and the icosahedral subgroups resulting from the symmetry-lowering distortions.

In the present paper we follow this line of attack to analyse the ground-state properties at strong coupling for $G\otimes(g \oplus h)$ and its two subsystems $G\otimes g$ and $G\otimes h$. We begin in section 4 with a treatment of $G\otimes(g \oplus h)$ with equal coupling, $G\otimes(g \oplus h)_{eq}$. We know from Pooler's work on continuous group invariances [3] that $G\otimes(g \oplus h)_{eq}$ has a continuous group invariance of SO(4). The resulting minimum-energy hypersphere in the nine-dimensional phase space may be conveniently parametrized in terms of spherical biharmonics [16]. This parametrization serves to facilitate the subsequent Berry phase [17, 18] analysis, the results of which are used to calculate the degeneracies [19], energies and Ham factors [20, 21] of the low-lying states at strong coupling. In section 5 the corresponding analysis is presented for the subsystems $G\otimes g$ and $G\otimes h$. In these two systems, the eigenstates in the minima of the corresponding lowest adiabatic potential energy sheets (called LAPES in what follows) no longer form a continuum but occur at discrete values of the biharmonic parameters. These points are related by the operations of the icosahedral subgroups resulting from the symmetry-lowering distortions. A *duality* between $G\otimes h$ and $H\otimes g$ is found to exist and we utilize it to obtain the ground-state properties in these two systems. Finally in section 6 we consider the Berry phases in $G\otimes(g \oplus h)$ at all relative coupling strengths of the g- and h-vibrations.

3. The Clebsch–Gordan coupling matrices

We begin by considering the Jahn–Teller matrix operator in the G basis. The Hamiltonian can be written as follows:

$$\mathcal{H} = -\frac{1}{2}\sum_{\Lambda,\lambda}\frac{\partial^2}{\partial Q_{\Lambda,\lambda}^2} + \frac{1}{2}\sum_{\Lambda,\lambda}\omega_\Lambda^2 Q_{\Lambda,\lambda}^2 + \mathcal{H}_{JT} \tag{1}$$

where $\mathcal{H}_{JT}$ is the Jahn–Teller interaction, which we write in a form that shows its derivation from the linear term in a Taylor expansion:

$$\mathcal{H}_{JT} = \sum_{\Lambda,\lambda}\left[\frac{\partial H}{\partial Q_{\Lambda,\lambda}}\right] Q_{\Lambda,\lambda} \tag{2}$$

$Q_{\Lambda,\lambda}$ here denotes one of the nine Jahn–Teller-active coordinates, ω_Λ^2 is the harmonic force constant for the Λ mode, and λ runs over its components. Λ may be G or H. Within the G electronic quartet the non-dynamic part of $\mathcal{H}$ yields an adiabatic potential surface comprising four sheets $E_k(Q)$,

$$E_k(Q) = \frac{1}{2}\sum_{\Lambda,\lambda}\omega_\Lambda^2 Q_{\Lambda,\lambda}^2 + \epsilon_k(Q) \qquad k = 1, 2, 3, 4 \tag{3}$$

where $\epsilon_k(Q)$ is the kth root of the secular equation:

$$|W_{ij}(Q) - \epsilon_k(Q)\delta_{ij}| = 0 \tag{4}$$

with

$$W_{ij}(Q) = \sum_{\Lambda,\lambda} \langle \mathrm{G}i | \frac{\partial H}{\partial Q_{\Lambda,\lambda}} | \mathrm{G}j \rangle Q_{\Lambda,\lambda} = \sum_{\Lambda,\lambda} k_\Lambda^{\mathrm{G}} Q_{\Lambda,\lambda} \langle \mathrm{G}i | \Lambda\, \lambda \mathrm{G}j \rangle. \tag{5}$$

k_Λ^{G} is the reduced matrix element for the operator of symmetry Λ. The Clebsch–Gordan coefficient $\langle \mathrm{G}i | \Lambda\, \lambda \mathrm{G}j \rangle$, is real and it is an element of a coupling matrix that represents the rule for constructing a rank-two symmetric tensor transforming as $|\Lambda\, \lambda\rangle$ from the components of a $|\mathrm{G}\rangle$ vector. This coupling matrix is the Jahn–Teller interaction for the $|\Lambda\, \lambda\rangle$ mode within the G electronic state. In all of the following we obtain these matrices by a method that we have found convenient and easy to make self-consistent. The method involves the calculation of all possible integrals of the form $\langle \mathrm{G}, i | Q_{\Lambda,\lambda} | \mathrm{G}, j \rangle$ with the aid of the *Mathematica* package. The Jahn–Teller interaction matrices that result are given in the appendix in a form that also serves to define the normalization and definition of the k_Λ^{G}s as we use them. The interaction matrices are, of course, determined purely by the symmetry, and could have been obtained by more obviously group theoretical methods, but we found the above method by far the quickest and most error-free. In the analysis of $\mathrm{G}\otimes(g \oplus h)_{\mathrm{eq}}$, the basis functions used to calculate the integrals come from the irreducible representations [1, 0] and [2, 0] of SO(4) (In the following we use Biedenharn's [22] designation of the irreducible representations of SO(4).) In the cases $\mathrm{G}\otimes g$, $\mathrm{G}\otimes h$ and $\mathrm{H}\otimes g$, the basis functions are derived from h and g of $\mathrm{I_h}$ subduced from SO(3) [2].

4. $\mathrm{G}\otimes(g\oplus h)_{\mathrm{eq}}$

The SO(4) invariance [3] of $\mathrm{G}\otimes(g \oplus h)_{\mathrm{eq}}$ is a convenient starting point for our analysis. At equal coupling, $\mathrm{G}\otimes(g\oplus h)$ becomes [1, 0]⊗[2, 0] of SO(4). In this case the minimum-energy surface of the LAPES is a continuous hyperspherical trough embedded in a nine-dimensional parameter space. The representation in electronic function space now becomes the SO(4) irrep [1, 0] [22]. Every antipodal pair of points on the unit hypersphere (S^3) representing [1, 0], corresponds to the same distortion in the vibrational coordinate space. Following the convention of Ceulemans [23], we denote the vibrational coordinate space with the letter v and the projective electronic function space with f.

4.1. The Jahn–Teller matrix for $G\otimes(g \oplus h)_{eq}$

Before we go into the construction of the Jahn–Teller matrices for $\mathrm{G}\otimes(g \oplus h)_{\mathrm{eq}}$ let us first consider the task of parametrizing the SO(4) group. There are two independent ways of doing this, corresponding to the two independent ways of parametrizing a four-dimensional Euclidean space in terms of angular coordinates. Bearing in mind that we require a parametrization that simplifies our analysis, we choose coordinates that have been termed *biharmonic* by Barut and Rączka [16] and utilizes

$$\begin{aligned} x_1 &= r\sin\theta\cos\alpha \qquad & x_2 &= r\sin\theta\sin\alpha \\ x_3 &= r\cos\theta\cos\beta \qquad & x_4 &= r\cos\theta\sin\beta \end{aligned} \tag{6}$$

which correspond to plane rotations in perpendicular spaces with $0 \leqslant r < \infty$, $0 \leqslant \alpha, \beta < 2\pi$, $0 \leqslant \theta < \pi/2$, the x_i being the cartesian coordinates in four dimensions. In terms of these coordinates the basis functions of the irreducible representations of SO(4), $[p, 0]$ with

$p = 0, 1, 2, \ldots$ may be expressed as hyperspherical biharmonics [16]. The general form of these biharmonics (unnormalized) for a given p is

$$Y^p_{m_1,m_2} = d^j_{\mu,\mu'}(2\theta)e^{im_1\alpha}e^{im_2\beta} \tag{7}$$

where the m_1 and m_2 are restricted by the following relation

$$|m_1| + |m_2| = p - 2s = 0, 1, \ldots, [p/2]. \tag{8}$$

The indices j, μ and μ' are defined as

$$j = \frac{p}{2} \qquad \mu = \frac{(m_2 + m_1)}{2} \qquad \mu' = \frac{(m_2 - m_1)}{2} \tag{9}$$

and the functions $d^j_{\mu,\mu'}(2\theta)$ are given by

$$d^j_{\mu,\mu'}(2\theta) = \sum_k F(j,k,\mu,\mu')(\cos\theta)^{2j+\mu-\mu'-2k}(\sin\theta)^{\mu'-\mu+2k} \tag{10}$$

with

$$F(j,k,\mu,\mu') = (-1)^{\mu'-\mu+k}\frac{\sqrt{(j+\mu)!(j-\mu)!(j+\mu')!(j-\mu')!}}{(j+\mu-k)!(j-\mu'-k)!k!(\mu'-\mu+k)!}. \tag{11}$$

In terms of these hyperspherical biharmonics the real electronic basis states ($|Gi\rangle$) belonging to [1, 0] (normalized to unity on S^3) may be written as

$$\begin{aligned} |G1\rangle &= \sqrt{\frac{2}{\pi^2}}\sin\theta\sin\alpha \qquad |G2\rangle = \sqrt{\frac{2}{\pi^2}}\sin\theta\cos\alpha \\ |G3\rangle &= \sqrt{\frac{2}{\pi^2}}\cos\theta\sin\beta \qquad |G4\rangle = \sqrt{\frac{2}{\pi^2}}\cos\theta\cos\beta. \end{aligned} \tag{12}$$

In terms of the coordinates $(q, \theta, \alpha, \beta)$, the nine normal mode vibrations (q_i) belonging to [2, 0] are

$$\begin{aligned} q_1 &= \frac{q}{\sqrt{3}}\cos 2\theta \qquad q_2 = \frac{q}{\sqrt{3}}\sin 2\theta\cos(\alpha+\beta) \\ q_3 &= \frac{q}{\sqrt{3}}\sin 2\theta\sin(\alpha+\beta) q_4 = \frac{q}{\sqrt{3}}\sin 2\theta\cos(\alpha-\beta) \\ q_5 &= \frac{q}{\sqrt{3}}\sin 2\theta\sin(\alpha-\beta) \qquad q_6 = q\sqrt{\frac{2}{3}}\sin^2\theta\cos 2\alpha \\ q_7 &= q\sqrt{\frac{2}{3}}\sin^2\theta\sin 2\alpha \qquad q_8 = q\sqrt{\frac{2}{3}}\cos^2\theta\cos 2\beta \\ q_9 &= q\sqrt{\frac{2}{3}}\cos^2\theta\sin 2\beta \end{aligned} \tag{13}$$

with $q^2 = \sum_\lambda q_\lambda^2$. With the above basis functions we calculate, using the method described in section 3, the linear coupling matrix for $G\otimes(g \oplus h)_{eq}$. We present the full form of this matrix, $||M^G([g \oplus h]_{eq})||$, together with its reduced matrix element k^G_{eq} in the appendix. Diagonalizing this matrix, we find a singlet state at an energy of $-3qk^G_{eq}$ below a triply degenerate state at an energy of $+qk^G_{eq}$, where k^G_{eq} is the linear Jahn–Teller coupling constant. In terms of the θ, α, β-parametrization, the eigenstate in f space corresponding to the singlet is

$$|\theta,\alpha,\beta\rangle = \sin\theta\sin\alpha|1\rangle + \sin\theta\cos\alpha|2\rangle + \cos\theta\sin\beta|3\rangle + \cos\theta\cos\beta|4\rangle \qquad \forall q. \tag{14}$$

Here the kets $|i\rangle$, $i = 1, 2, 3, 4$, are the G electronic unit vectors. The adiabatic potentials in v space are just the eigenvalues of the matrix $||M^{G}([g \oplus h]_{eq})||$ added to $q^2/2$. In terms of the coordinates $(q, \theta, \alpha, \beta)$, the LAPES has the very simple form

$$\frac{q^2}{2} - 3qk_{eq}^{G}. \tag{15}$$

4.2. The vibronic ground state on the LAPES.

On the LAPES we are looking for a vibronic ground state of the form used in the adiabatic approximation:

$$\Psi = \psi(q, \theta, \alpha, \beta)u(q, \theta, \alpha, \beta, r) \tag{16}$$

where r represents all the electronic coordinates. Here u is the state given in equation (14). If we substitute this solution into the Schrödinger equation of motion on the LAPES, making the usual adiabatic approximation, we obtain

$$-\frac{1}{2}[u\nabla^2\psi + 2\nabla\psi \cdot \nabla u + \psi\nabla^2 u] + \left(\frac{q^2}{2} - 3qk_{eq}^{G}\right)\psi u = E\psi u \tag{17}$$

where ∇ is the usual momentum operator in the coordinate representation. Applying closure with u to this equation yields

$$-\frac{1}{2}\nabla^2\psi - \nabla\psi \cdot \langle u|\nabla u\rangle - \frac{1}{2}\psi\langle u|\nabla^2 u\rangle + \left(\frac{q^2}{2} - 3qk_{eq}^{G}\right)\psi = E\psi. \tag{18}$$

The components of ∇ in the biharmonic coordinate representation are

$$\left(\frac{\partial}{\partial q}, \frac{1}{q}\frac{\partial}{\partial\theta}, \frac{1}{q\sin\theta}\frac{\partial}{\partial\alpha}, \frac{1}{q\cos\theta}\frac{\partial}{\partial\beta}\right). \tag{19}$$

We may now calculate the terms in equation (18) and we obtain

$$\langle u|\nabla u\rangle = \mathbf{0} \tag{20}$$

as is always the case if $|u\rangle$ is real and normalized. The Laplace–Beltrami operator, ∇^2, in terms of the biharmonic coordinates is as follows:

$$\frac{1}{q^3}\frac{\partial}{\partial q}q^3\frac{\partial}{\partial q} + \frac{1}{q^2\sin\theta\cos\theta}\frac{\partial}{\partial\theta}\sin\theta\cos\theta\frac{\partial}{\partial\theta} + \frac{1}{q^2\sin^2\theta}\frac{\partial^2}{\partial\alpha^2} + \frac{1}{q^2\cos^2\theta}\frac{\partial^2}{\partial\beta^2}. \tag{21}$$

The second term of equation (18) may now be calculated yielding

$$\langle u|\nabla^2 u\rangle = -\frac{3}{q^2}. \tag{22}$$

Equation (18) then becomes

$$-\frac{1}{2}\frac{1}{q^3}\frac{\partial}{\partial q}q^3\frac{\partial}{\partial q}\psi - \frac{\Delta(\theta, \alpha, \beta)}{2q^2}\psi + \frac{3}{2q^2}\psi + \left(\frac{q^2}{2} - 3qk_{eq}^{G}\right)\psi = E\psi \tag{23}$$

where $\Delta(\theta, \alpha, \beta)$ is the angular part of the operator in (21). The LAPES here, given by equation (15), may be thought of as a hyperspherical 'trough' of radius $3k_{eq}^{G}$ and depth $\approx 9(k_{eq}^{G})^2/2$ embedded in the nine-dimensional parameter space. When the 'trough' is deep the wave function for the low-lying vibronic states will be concentrated on the hyperspherical continuum of minima, the distance from the next triply degenerate APES will be large $12(k_{eq}^{G})^2$, and the conditions for application of the adiabatic approximation will be satisfied. The appropriate concentration of wave function in the 'trough' occurs when we separate the variables and extract a radial part that is a harmonic oscillator wave function centred on

the minimum hypersurface at $q \approx 3k_{eq}^{G}$. Factorizing out the q-dependence leaves us with an equation in θ, α and β of the form

$$\Delta(\theta, \alpha, \beta) f(\theta, \alpha, \beta) + \gamma f(\theta, \alpha, \beta) = 0 \tag{24}$$

where γ is a constant. This equation of motion over the minimum-energy hypersurface is quite straightforward to solve by first substituting periodic α- and β-dependences of period 2π. Appropriate factors are of the form $\exp(im_1\alpha)$ and $\exp(im_2\beta)$ with integral m_1 and m_2. On making this substitution and setting $\gamma = l(l+2)$ we see that this equation is the equation discussed by Barut and Rączka [16] in their treatment of harmonic functions for SO(N) [16] in the case of SO(4). The second-order ordinary differential equation resulting from the above manipulations is

$$\left[\frac{1}{\sin\theta\cos\theta}\frac{d}{d\theta}\sin\theta\cos\theta\frac{d}{d\theta} - \frac{m_1^2}{\sin^2\theta} - \frac{m_2^2}{\cos^2\theta} + l(l+2)\right]\Theta^{l}_{m_1,m_2}(\theta) = 0 \tag{25}$$

where $\Theta^{l}_{m_1,m_2}(\theta)$ is the θ-dependence of the nuclear wave functions which may be written in terms of hypergeometric functions as follows:

$$\Theta^{l}_{m_1,m_2}(\theta) = \tan^{m_1}\theta\cos^{l}\theta \times {}_2F_1\left[\frac{1}{2}(|m_1| - l + m_2), \frac{1}{2}(|m_1| - l + m_2); m_1 + 1; -\tan^2\theta\right] \tag{26}$$

where l, m_1 and m_2 are restricted by the condition that $\Theta^{l}_{m_1,m_2}(\theta)$ is a square integrable function with respect to the measure $\sin\theta\cos\theta\ d\theta\ d\alpha\ d\beta$, i.e.

$$|m_1| + |m_2| = l - 2s \qquad s = 0, 1, \ldots, [l/2]. \tag{27}$$

These are exactly the same restrictions as those on the indices of the spherical biharmonics in equation (7) with $p = l$. In fact, the $\Theta^{l}_{m_1,m_2}(\theta)$ may be expressed in terms of the $d^{j}_{\mu,\mu'}$-functions. The orthonormal basis of the corresponding Hilbert space, $H^{l}(S^3)$, of nuclear motion on or near the minimum-energy hypersurface is then given by the spherical biharmonics of equation (7). These are the bases of the SO(4) irreducible representations $[l, 0]$ for $l = 0, 1, 2, 3, \ldots$. The degeneracies are $(l+1)^2$, as can be found from the SO(3) subduction of these SO(4) representations. The resulting eigenvalues of equation (23) are then, to order $(1/k_{eq}^{G})^2$,

$$E = -\frac{9}{2}(k_{eq}^{G})^2 + \frac{1}{2} + \left(\frac{l(l+2)}{9} - \frac{5}{24}\right)/(k_{eq}^{G})^2. \tag{28}$$

This is still not the total energy, because we have left out five of the nine degrees of freedom in concentrating on the SO(4) sub-space, but at equal coupling none of these extra degrees of freedom couple linearly to the electronic states, so they only contribute a zero-point energy of $5/2$ to E.

4.2.1. Berry phase changes over the LAPES. There is one final restriction that has to be applied to the functions in (26) before they can properly represent the nuclear wave functions of this problem. The total vibronic wave function is the product of a nuclear wave function and a vector u in f space. Physically, if we transport the system around an adiabatic circuit in parameter space, the total vibronic wave function must remain unchanged. The vector u however, suffers a Berry phase change of π over the same circuit. More precisely, antipodal pairs of points $((\theta, \alpha, \beta)$ and $(\theta, \alpha + \pi, \beta + \pi))$ in f space represent the same distortion in v space. Therefore, the vibronic wave function will remain unchanged only if the nuclear wave functions suffer the same phase change as that of the u vector. This

means that only the irreducible representations $[l, 0]$ for $l = 1, 3, 5, \ldots$ of SO(4) properly describe the angular dependences of the nuclear wave functions. The lowest vibronic state has therefore a fourfold degeneracy corresponding to the nuclear motion state $[1, 0]$. We thus recover the result that is characteristic of the Jahn–Teller effect; that is, when proper account of the Berry phase is taken, the lowest vibronic state has the same degeneracy as the original electronic state that couples to the vibrations.

4.2.2. The Ham factors within the vibronic ground state. We now proceed to calculate the Ham factors for the operators that transform according to $[2, 0]$ of SO(4) (i.e. $g \oplus h$ of the icosahedral group at equal coupling) within the vibronic ground state. A general definition of a Ham factor is

$$K(\Gamma) = \frac{\langle \Phi_i | V^\Gamma | \Phi_j \rangle}{\langle \psi_i^{\mathrm{el}} | V^\Gamma | \psi_j^{\mathrm{el}} \rangle} \tag{29}$$

where ψ^{el}s are members of the original electronic basis set, the Φs are the vibronic ground states, and V^Γ is an operator transforming according to the irreducible representation Γ operating in F space. In the limit of strong coupling, the vibronic ground state obtained above may be written as

$$\Phi_k = \frac{1}{q\sqrt{q}} Q(q - 3k_{\mathrm{eq}}^{\mathrm{G}}) \Omega_k(\theta, \alpha, \beta) |u\rangle \tag{30}$$

where $Q(q - 3k_{\mathrm{eq}}^{\mathrm{G}})$ is a normalized harmonic oscillator wave function centred at $q = 3k_{\mathrm{eq}}^{\mathrm{G}}$, the $\Omega_k(\theta, \alpha, \beta)$ are the $|G_k\rangle$ of equation (12) for $k = 1, 2, 3, 4$, and $|u\rangle$ is the ket given in equation (14). To calculate the Ham factor $K(\Gamma)$, we first calculate the expectation value of V^Γ within the electronic state $|u\rangle$ and then the expectation of the resulting function within the nuclear wave functions $\Omega_k(\theta, \alpha, \beta)$. For $\Gamma = [2, 0]$, our choice of $V^{(\Gamma=[2,0])}$ is the matrix in appendix A, equation (A1), with $q_1 = 1$ and $q_i = 0$ with $i = 2, 3, \ldots$, although the calculation would of course yield the same Ham factor for any operator transforming as $[2, 0]$. Let this matrix be $||c_1||$. Following the procedure above, the expectation of this matrix within $|u\rangle$ is $\cos 2\theta$, and the expectation of this within the $\Omega_k(\theta, \alpha, \beta)$ is the 4×4 matrix $(1/3)||c_1||$. The Ham factor at strong coupling for the equally coupled g- and h-vibrations within the vibronic ground state is therefore

$$K([2, 0]) = \frac{1}{3}.$$

The two Ham factors of the antisymmetric operators, T_1 and T_2, in this vibronic ground state are necessarily zero.

5. G⊗*g*, G⊗*h* and H⊗*g*

The topologies of the APESs for these three subsystems have already been studied in the work of Ceulemans *et al* [9, 10]. However, no treatment of the Berry phase and its consequences on the ordering of the low-lying energy levels was done. To do this we started, following Khlopin *et al* [11], by using the analytic method devised by Öpik and Pryce (see [24], equations 10), to find the extrema on the APESs. With the aid of the *Mathematica* package this procedure is very fast and easily implemented.

Ceulemans [23] showed the equivalence of the Öpik and Pryce method to his use of isostationary functions and the *epikernel principle* [15]. In the f space representation of

G⊗g, the minima and saddles occur at points corresponding respectively to the maximal and lower ranking epikernels. The same is true of the v-space representation of this scheme. However, in the v representation the positions of the extrema are not projected onto a unit hypersphere. In the v representation the extrema are distributed in phase space on concentric hyperspheres, each hypersphere corresponding to one type of extremum. The angular coordinates of the extrema over these hyperspheres are the same as those of the f-space representation. In a similar way, we find later that G⊗h and H⊗g share a common maximal epikernel symmetry for minima (see the genealogy in figure 2 of [9]). The f representation of G⊗h minima is therefore just a projective version of the v representation of H⊗g minima and vice versa. With this in mind, we call G⊗g, *self-dual* and G⊗h, *dual* to H⊗g, with respect to minima.

5.1. The bases used to calculate the coupling matrices for G⊗g, G⊗h and H⊗g

To calculate the coupling matrices for these systems we chose as far as possible to use the functions that were earlier used in [11]. The H and G bases are taken respectively from the $J = 2$ and $J = 3$ irreps of SO(3). The functions representing the vibrational modes h and g have to be even and come from the SO(3) irreps $J = 2$ and $J = 4$ respectively. The symmetries of these bases and normal modes are listed below in Cartesian coordinates with the equality sign taken to mean *transforms as*.

(i) Quintet modes and bases. The $J = 2$ irrep of the SO(3) group reduces exactly to H [2]. Thus functions transforming according to H may be written exactly as a set of d states:

$$\begin{aligned} &qh_1, \ |\mathrm{H1}\rangle = 2x^2 - x^2 - y^2 \\ &qh_2, \ |\mathrm{H2}\rangle = zx \\ &qh_3, \ |\mathrm{H3}\rangle = xy \\ &qh_4, \ |\mathrm{H4}\rangle = x^2 - y^2 \\ &qh_5, \ |\mathrm{H5}\rangle = yz. \end{aligned} \tag{31}$$

(ii) Quartet modes and bases. Where an irrep of SO(3) splits into more than one irrep of the icosahedral group, a general method for finding the bases is to diagonalize an operator of icosahedral symmetry in the angular momentum eigenstates. All the necessary information for this is given by Judd [2]. A suitable operator, in Cartesian coordinates with the fivefold axis along Oz, is

$$V_{\mathrm{icos}} = 231z^6 - 315r^2z^4 + 105r^4z^2 - 5r^6 + 42z(x^5 - 10x^3y^2 + 5xy^4). \tag{32}$$

Since we do not require that the electronic bases be even, we may take the G states that first appear in the $J = 3$ irrep of SO(3). $J = 3$ is shared with the T_2 irrep, and diagonalizing V_{icos} in $J = 3$ sorts out the quartet from the triplet states. This quartet basis, which is also used in [11], is

$$\begin{aligned} |\mathrm{G1}\rangle &= y^3 - 3x^2y - 4xyz \\ |\mathrm{G2}\rangle &= x^3 - 3xy^2 - 2x^2z + 2zy^2 \\ |\mathrm{G3}\rangle &= y(r^2 - 5z^2) \\ |\mathrm{G4}\rangle &= x(5z^2 - r^2). \end{aligned} \tag{33}$$

The vibrational mode symmetries, being even, are obtained from a diagonalization of V_{icos}

in $J = 4$. The quartet modes are

$$\begin{aligned} qg_1 &= (x^2 - y^2)(x^2 + y^2 - 6z^2) - z(3y^2x - x^3) \\ qg_2 &= -2xy(x^2 + y^2 - 6z^2) + z(3x^2y - y^3) \\ qg_3 &= -xz(3x^2 + 3y^2 - 4z^2) + x^4 + y^4 - 6x^2y^2 \\ qg_4 &= -yz(3x^2 + 3y^2 - 4z^2) - 4yx(x^2 - y^2). \end{aligned} \tag{34}$$

The interaction matrices for G⊗g, G⊗h and H⊗g are respectively denoted $||M^{G}(g)||$, $||M^{G}(h)||$ and $||M^{H}(g)||$. They are obtained from the transformation properties of the above functions. These matrices are listed in appendix A.

5.2. *The method of Öpik and Pryce.*

5.2.1. G⊗g and G⊗h. In terms of our notation, this method requires us to solve the following set of equations in terms of $||M||$, one of the matrices in the preceding section, a, a normalized column vector of the dimension of $||M||$, and $\{q_i\}$, the set of normal-mode coordinates in $||M||$.

$$\begin{aligned} &||M||a = Ea \\ &a^{T}\left(\frac{\partial||M||}{\partial q_i}\right)a + \omega_{\Lambda}^2 q_i = 0 \\ &a^{T}a = 1 \end{aligned} \tag{35}$$

where $||M||$ is assumed to contain the reduced matrix element k_{Λ} in the form given in appendix A. This procedure finds the eigenvector a of the Jahn–Teller matrix $||M||$ that corresponds to a turning point of the appropriate APES. Below, we tabulate the results obtained from the Öpik and Pryce analysis on G⊗g and G⊗h. The results are given as positions on the f-space hypersphere (θ, α, β). The antipodal equivalent of (θ, α, β) is at $(\theta, \bar{\alpha}, \bar{\beta})$ where $\bar{\alpha}, \bar{\beta}$ is taken to mean $\alpha + \pi, \beta + \pi$. The eigenstates corresponding to these f-space points are given by equation (14). In table 1, the columns marked $E(G \otimes g)$ and $E(G \otimes h)$ show the energy at the particular extremum type.

Table 1.

Symmetry	$E(G \otimes g)$	$E(G \otimes h)$	$(\theta, \alpha/(\pi/10), \beta/(\pi/10))$
D_{3h}(I)	$-6(k_g^G)^2/\omega_g^2$	$-3(k_h^G)^2/\omega_h^2$	$(\theta_1^{(1)}, 0, 0)$, $(\theta_1^{(1)}, 8, \bar{6})$, $(\theta_1^{(1)}, 6, 2)$, $(\theta_1^{(1)}, \bar{4}, \bar{8})$, $(\theta_1^{(1)}, \bar{2}, 4)$ $(\theta_2^{(1)}, 0, \bar{0})$, $(\theta_2^{(1)}, 8, 6)$, $(\theta_2^{(1)}, 6, \bar{2})$, $(\theta_2^{(1)}, \bar{4}, 8)$, $(\theta_2^{(1)}, \bar{2}, \bar{4})$
D_{2h}(II)	$-(k_g^G)^2/\omega_g^2$	$-8(k_h^G)^2/\omega_h^2$	$(\theta_1^{(2)}, 0, 0)$, $(\theta_1^{(2)}, \bar{8}, 6)$, $(\theta_1^{(2)}, \bar{2}, 4)$, $(\theta_1^{(2)}, \bar{6}, \bar{2})$, $(\theta_1^{(2)}, \bar{4}, \bar{8})$ $(\theta_2^{(2)}, \bar{0}, 0)$, $(\theta_2^{(2)}, 8, 6)$, $(\theta_2^{(2)}, 2, 4)$, $(\theta_2^{(2)}, \bar{6}, 2)$, $(\theta_2^{(2)}, \bar{4}, 8)$ $(\pi/4, 5, 5)$, $(\pi/4, 7, 1)$, $(\pi/4, \bar{7}, 9)$, $(\pi/4, \bar{1}, 7)$, $(\pi/4, \bar{9}, 3)$
D_{3h}(III)	$-\frac{2}{3}(k_g^G)^2/\omega_g^2$	$-\frac{25}{3}(k_h^G)^2/\omega_h^2$	$(\theta_1^{(3)}, 9, \bar{3})_1$, $(\theta_1^{(3)}, 7, \bar{9})_2$, $(\theta_1^{(3)}, \bar{5}, \bar{5})_3$, $(\theta_1^{(3)}, 3, \bar{1})_4$, $(\theta_1^{(3)}, \bar{1}, 7)_5$ $(\theta_2^{(3)}, 9, \bar{3})_6$, $(\theta_2^{(3)}, \bar{7}, 9)_7$, $(\theta_2^{(3)}, 5, 5)_8$, $(\theta_2^{(3)}, \bar{3}, 1)_9$, $(\theta_2^{(3)}, \bar{1}, 7)_{10}$
T_h(IV)	$-9(k_g^G)^2/\omega_g^2$	0	$(\pi/4, \bar{5}, 5)_1$, $(\pi/4, 7, 9)_2$, $(\pi/4, 3, 1)_3$, $(\pi/4, \bar{1}, \bar{7})_4$, $(\pi/4, \bar{9}, \bar{3})_5$

with

$$\theta_1^{(1)} = \Omega_I/2 \qquad \theta_1^{(2)} = \pi/4 + \Omega_I/2 \qquad \theta_1^{(3)} = \pi/2 - \theta_2^{(3)}$$
$$\theta_2^{(1)} = \pi/2 - \theta_1^{(1)} \qquad \theta_2^{(2)} = \pi/2 - \theta_1^{(2)} \qquad \theta_2^{(3)} = \Omega_D/2$$

where Ω_I is the icosahedral angle between two neighbouring fivefold axes: $\tan\Omega_I = 2$; and Ω_D is the dodecahedral angle between two neighbouring threefold axes: $\cos\Omega_D = (\sqrt{5}-1)/2\sqrt{3})$. In table 1, our designation of the extremum types may be related to that of Ceulemans *et al* [9] via: (I)→ γ, (II)→ δ, (III)→ β, (IV)→ α, and the numbering of individual extrema is as in appendix A. It should be noted that the type (III) extrema in G⊗g do not occur on the LAPES and we underline the corresponding energy to emphasize this. The nature of the extrema (I–IV) depends on the interaction. In G⊗g, the maximal epikernels are T_h, D_{3h} and D_{5h} and further analysis of the curvature at these points on the LAPES shows that the stable minima occur at type (IV) points (T_h). The nearest saddles occur at type (I) points (D_{3h}) and are on the lowest-energy paths between the type (IV) minima. The idea that extrema prefer to lie on maximal epikernel points is a conclusion that one could have arrived at through the epikernel principle [15]. In the case of G⊗h, the positions of the stable minima once again agree with the epikernel principle [15], as do the other extrema. In G⊗h, the minima are the type (III) extrema. The nearest saddles are the type (II) extrema and are on the lowest-energy paths between the type (III) minima. In table 1 we have numbered the states that correspond to stable minima so that in later calculations individual minima may be identified easily.

Let us now turn our attention to the v-space representation of the distorted configurations. The second equation in (35), gives us the v-space coordinates of the extrema. Let us consider a minimum m in the coupling scheme $\Gamma \otimes \Lambda$ with f-space coordinates given by the set of four numbers $\{a_i^\Gamma(m)\}$, $i = 1, 2, 3, 4$. We tabulate our v-space representations by constructing a matrix with elements, $||Q_{m,n}^{\Gamma\Lambda}||$, given by:

$$||Q_{m,n}^{\Gamma\Lambda}|| = -(a^\Gamma(m))^T \left(\frac{\partial||M^\Gamma(\Lambda)||}{\partial q\lambda_n}\right) a^\Gamma(m). \tag{36}$$

The rows of this matrix are labelled by the different minima (m) and the columns are labelled by the different basis distortions $\{q\lambda_n\}$. The corresponding matrices for G⊗g and G⊗h are then

$$\begin{aligned} ||Q_{m,n}^{Gg}|| &= -(a^G(m))^T \left(\frac{\partial||M^G(g)||}{\partial q g_n}\right) a^G(m) \qquad m = 1,2,3,4,5,\ n = 1,2,3,4 \\ ||Q_{m,n}^{Gh}|| &= -(a^G(m))^T \left(\frac{\partial||M^G(h)||}{\partial q h_n}\right) a^G(m) \qquad m = 1,2,\ \ldots,\ 10,\ n = 1,2,\ \ldots,\ 5 \end{aligned} \tag{37}$$

and they are given explicitly in appendix B. The minima (m) are as listed in table 1.

5.2.2. H⊗g. The method of Öpik and Pryce is difficult to use for this case because there are five a_i to be found, and our use of it did not produce any minimum points at all. It only produced some turning points at T_h symmetry, which turned out to be degenerate on closer inspection. However, a numerical search over the H⊗g LAPES shows that this surface has stable minima at points of D_{3h} symmetry. This is the duality mentioned earlier between G⊗h and H⊗g. G⊗h and H⊗g share a common maximal epikernel symmetry for minima (D_{3h}), so the coordinates $\{a_i^H(m)\}$, $i = 1, 2, 3, 4, 5$, for a minimum m in H⊗g, are just the $||Q_{m,i}^{Gh}||$ projected onto a five-dimensional unit sphere. The $||Q||$ matrix elements for H⊗g are then

$$||Q_{m,n}^{Hg}|| = -(a^H(m))^T \left(\frac{\partial||M^H(g)||}{\partial q g_n}\right) a^H(m) \qquad m = 1,2,\ldots,10,\ n = 1,2,3,4 \tag{38}$$

(appendix B). In subsection 5.3 we use these matrices to obtain orthogonal transformations, $\mathbf{T}(T_h)$ and $\mathbf{T}(D_{3h})$, that reduce the spaces of T_h (G⊗g) and D_{3h} (G⊗h and H⊗g) minima into irreducible spaces of the icosahedral group.

5.3. The transformations $\mathbf{T}(T_h)$ *and* $\mathbf{T}(D_{3h})$.

The v representation of a Jahn–Teller system is just a state space of all possible distortions that may be reached by the Jahn–Teller-active coordinates. For a given coupling scheme, the distortion state at any point, v_0, in v space may be represented as a linear combination of the basis kets of v. The coefficients of this linear combination are just the values of the vibration coordinates at v_0. The matrices of these coefficients for G⊗g, G⊗h and H⊗g are given in equations (37), (38) and in appendix B. First let us consider the simplest case, G⊗g. The matrix of coefficients, $||Q^{Gg}||$, is a 4×5 matrix that describes how to construct states of T_h symmetry out of G basis states. This matrix, when column normalized, forms part of a full orthogonal transformation that transforms the static† representation of minima, into irreps of the icosahedral group. The full orthogonal transformation is then a 5×5 matrix with a 4×5 section containing the elements of the column-normalized $||Q^{Gg}||$. The remaining 1×5 section is the normalized column vector, $\sqrt{1/5}(1, 1, 1, 1, 1)$. This is the orthogonal transformation, $\mathbf{T}(T_h)$, that reduces the space of T_h minima of G⊗g, into irreducible spaces A and G of the icosahedral group. In the same way we may proceed to the construction of the corresponding transformation for the minima of G⊗h and H⊗g, $\mathbf{T}(D_{3h})$. This orthogonal transformation is a 10×10 matrix with a 4×10 section containing the elements of the column-normalized matrix $||Q^{Hg}||$ and a 5×10 section containing the elements of the column-normalized matrix $||Q^{Gh}||$. The remaining 1×10 section is the normalized column vector, $\sqrt{1/10}(1, 1, 1, 1, 1, 1, 1, 1, 1, 1)$. $\mathbf{T}(D_{3h})$ thus reduces the space of D_{3h} minima of G⊗h and H⊗g, into irreducible spaces A, G and H of the icosahedral group.

5.4. The Berry phase on the LAPES *and the tunnel splitting of the Jahn–Teller ground states*

Thus far we have been studying the static Jahn–Teller effect in G⊗g, G⊗h and H⊗g. In this section we look at what happens if a small amount of tunnelling is allowed for in the calculation of energies. The tunnelling restores the full icosahedral symmetry of the Jahn–Teller system and a splitting of the static ground state occurs. How the resulting split is ordered can be deduced from an analysis of the Berry phase on the corresponding LAPES.

5.4.1. Numerical phase tracking. Since the Jahn–Teller matrices are being diagonalized numerically, the phases of the eigenvectors must also be tracked numerically. This is a little tricky because there is no intrinsic way of relating the phase of an eigenvector calculated at two neighbouring points on the LAPES. A method that we found very easy to use is that of adjusting the overall sign of each eigenvector so that the first component is always positive. This produces continuity except where the first component would naturally go through zero. We then plot the components of the eigenvectors and count the number of discontinuities which should of course occur at the same point for each component. If this number is odd then the eigenstate will have changed sign an odd number of times implying an overall Berry phase change of π on completion of the adiabatic loop. Examples of this phase tracking for paths on the LAPES of G⊗h are given in figure 1. Below we treat the phase tracking in the three cases G⊗g (A), G⊗h (B) and H⊗g (C).

† In the first instance we are dealing only with the static Jahn–Teller effect where we do not take into account tunnelling between minima.

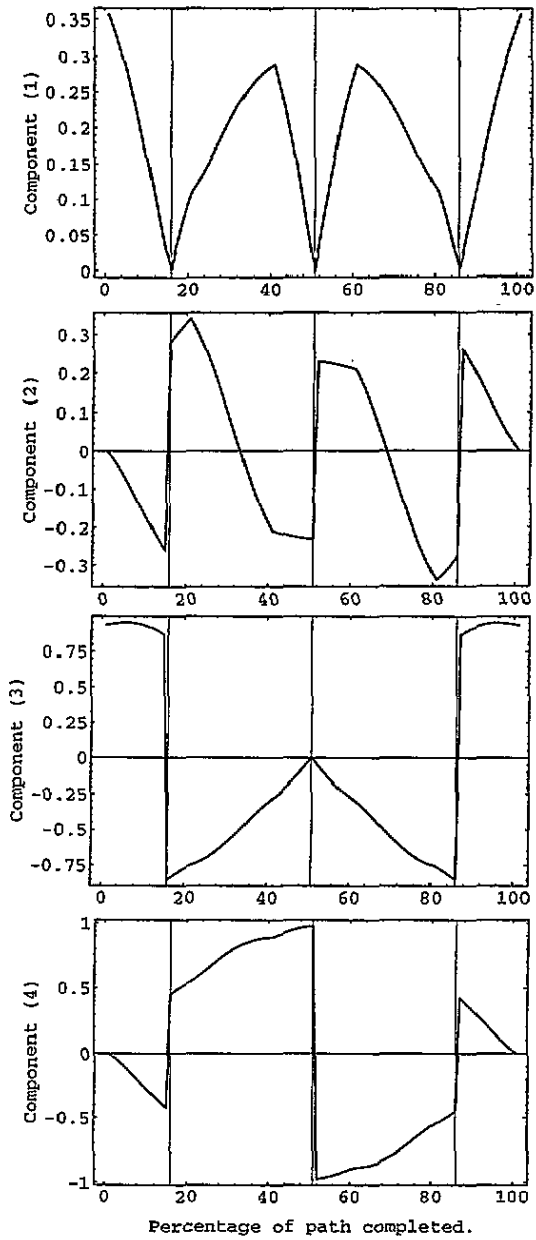

Figure 1. Four plots that show the tracking of the four components of an electronic eigenstate around a closed path in v space. On this path the plots make it obvious that three sign changes will ensure continuity, so there is a phase change of π around the complete path.

(A) G⊗g. We use the biharmonic parametrization to map out the LAPES of G⊗g (see equations (12)):

$$\begin{aligned} qg_1 &= q\sin\theta\sin\alpha \\ qg_2 &= q\sin\theta\cos\alpha \\ qg_3 &= q\cos\theta\sin\beta \\ qg_4 &= q\cos\theta\cos\beta. \end{aligned} \tag{39}$$

Everything can then be plotted in the sub-space q = constant. The minima all occur at $\theta = \pi/4$, so we take that as defining a base plane and plot α and β along cartesian axes in this plane. Because of the periodicity in α and β, this has the effect of plotting this sub-space onto a unit cell of a two-dimensional cubic lattice. This base plane also contains the points where the LAPES is triply degenerate. These points correspond to distortions of tetragonal symmetry of opposite sign to those giving minima, and on our base plane they appear at the face centres of the lattice of minima. To get the rest of the sub-space we plot θ along the vertical axis perpendicular to the base plane. In figure 2. we plot the gap between the two lowest eigenvalues of $||M^{G}(g)||$ across this base plane, and the minima and threefold-degeneracy points are clearly visible.

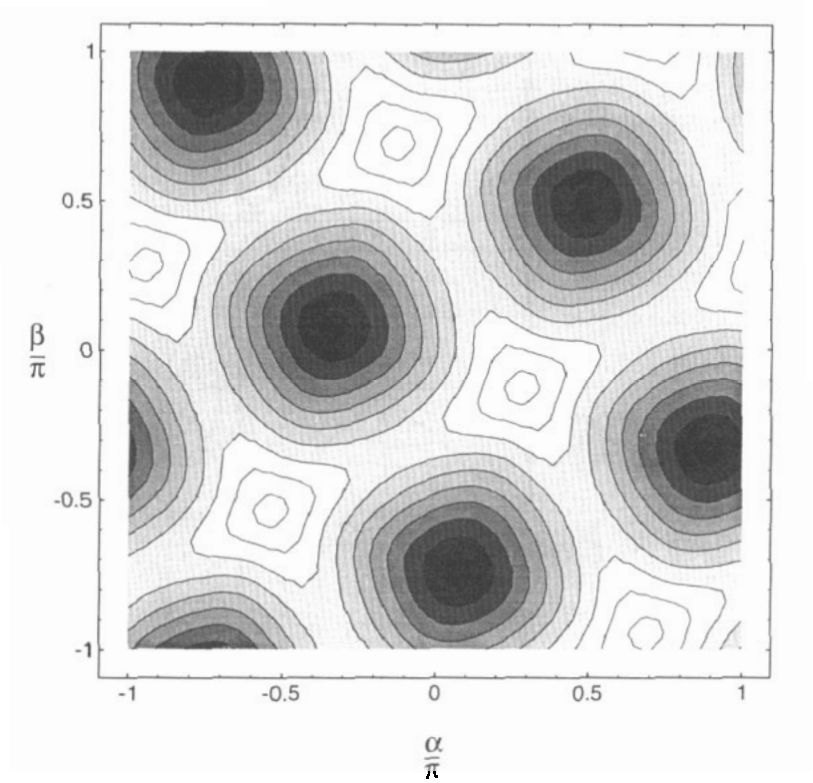

Figure 2. A contour plot of the difference in energy between the two lowest APESs for G⊗g. The minima appear as circular wells and the threefold degeneracies as squarish peaks.

The nature of the degeneracies is studied by taking a new origin at one of them, and manipulating the resulting form of $||M^{G}(g)||$ to show that near the origin it has exactly the same form as the matrix for the Jahn–Teller interaction T⊗τ_2, so we know that four lines of degeneracy radiate from it towards the vertices of a tetrahedron, two above the base plane and two below it [25].

Next we turn our attention to the saddle points. These are all to be found at points with the same value of $|\theta - \pi/4|$, half with $\theta > \pi/4$ and half with $\theta < \pi/4$,and with values of α and β that correspond to points on the base plane that are halfway between neighbouring minima as well as being halfway between neighbouring threefold-degeneracy points. Wherever a saddle point is at such a point above the base plane, there is a twofold

degeneracy at the mirror image point below the base plane. All these points correspond to distortions of the icosahedron of D_{3h} symmetry (type (I), see table 1). These twofold degeneracies lie on lines of degeneracy that go from one threefold point to the next, half of them looping above the base plane and half of them looping below the base plane. A numerical scan of the difference between the two lowest eigenvalues of $||M_g^G||$ across planes above and below the base plane picks up these lines of degeneracy again and shows where they go (figure 3).

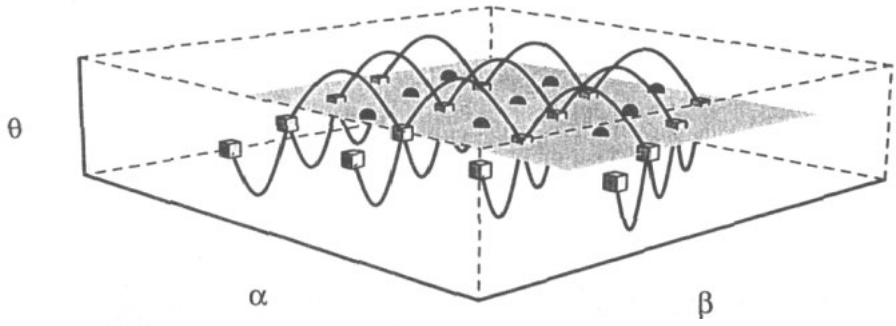

Figure 3. This figure shows, schematically, the lines of degeneracy above and below the plane $\theta = \pi/4$ for G⊗g. Cubes mark points of threefold degeneracy and dots mark positions of minima.

Using the phase-tracking method just described, we find various adiabatic loops that produce Berry phase changes in the eigenvector. One set are paths that go from $\beta = -\pi$ to $\beta = \pi$ holding α constant. This type of path can be understood if we consider joining the two ends, which are at the same point in phase space, by rolling up the unit cell, and counting the number of lines of degeneracy that are enclosed by the cylinder. We should recall that for real states in a many-dimensional phase space, tracking the phase around a closed loop produces a phase change of π for every line of degeneracies that intersects the loop [17, 18]. The two real eigenvectors of opposite sign corresponding to each of the minima in v space appear as a pair of antipodal eigenstates in f space. For the eigenstate at the ith minimum $|m_i\rangle$ we call its antipodal equivalent $|\bar{m}_i\rangle$. The upshot of the phase studies is that a consistent account of the relative phases may be produced if we implement the following rule: As one transports an eigenstate on the G⊗g LAPES from the ith to jth to kth to ... minima, the eigenstate passes from $|m_i\rangle$ to $|\bar{m}_j\rangle$ to $|m_k\rangle$ to ... eigenstates.

(B) G⊗h. For this case we parametrize the LAPES in terms of the coordinates $\{Q, \alpha, \gamma, \theta, \phi\}$ [26] as follows:

$$
\begin{aligned}
qh_1 &= Q((1/2)(3\cos^2\theta - 1)\cos\alpha + (1/2)\sqrt{3}\sin^2\theta\sin\alpha\sin 2\gamma) \\
qh_2 &= Q((1/2)\sqrt{3}\sin 2\theta\cos\phi\cos\alpha - (1/2)\sin 2\theta\cos\phi\sin\alpha\cos 2\gamma \\
&\qquad + \sin\theta\sin\phi\sin\alpha\sin 2\gamma) \\
qh_3 &= Q((1/2)\sqrt{3}\sin^2\theta\sin 2\phi\cos\alpha + (1/2)(1+\cos^2\theta)\sin 2\phi\sin\alpha\cos 2\gamma \\
&\qquad + \cos\theta\cos 2\phi\sin\alpha\sin 2\gamma) \qquad (40) \\
qh_4 &= Q((1/2)\sqrt{3}\sin^2\theta\cos 2\phi\cos\alpha + (1/2)(1+\cos^2\theta)\cos 2\phi\sin\alpha\cos 2\gamma \\
&\qquad - \cos\theta\sin 2\phi\sin\alpha\sin 2\gamma) \\
qh_5 &= Q((1/2)\sqrt{3}\sin 2\theta\sin\phi\cos\alpha - (1/2)\sin 2\theta\sin\phi\sin\alpha\cos 2\gamma \\
&\qquad - \sin\theta\cos\phi\sin\alpha\sin 2\gamma)
\end{aligned}
$$

where $0 \leqslant Q < \infty$, $0 \leqslant \alpha < \pi/3$, $0 \leqslant \gamma < \pi$, $0 \leqslant \theta < \pi/2$, $0 \leqslant \phi < 2\pi$, so that all possible distortions in the five-dimensional phase space are covered. One may construct a third-order invariant [27], I, in terms of the $\{qh_i\}$, as shown below; this is greatly simplified in terms of the above parametrization:

$$I = qh_1(qh_1^2 - 3qh_4^2 - 3qh_3^2 + \frac{3}{2}qh_2^2 + \frac{3}{2}qh_5^2)$$
$$+3\sqrt{3}(qh_3qh_2qh_5 + \frac{1}{2}qh_4qh_2^2 - \frac{1}{2}qh_4qh_5^2) = Q^3\cos 3\alpha. \tag{41}$$

Finding that $\alpha = 0$ for one minimum, we use the above invariant to deduce that the α-value for all the minima is zero. This means that the positions of the minima only have a dependence on θ, ϕ . If we double the θ-range, the dependence on θ, ϕ is consistent with placing two copies of the same minima at the vertices of a dodecahedron embedded in the full five-dimensional parameter space. A plot of the energy of the LAPES projected onto the $\alpha = 0$ surface is shown in figure 4.

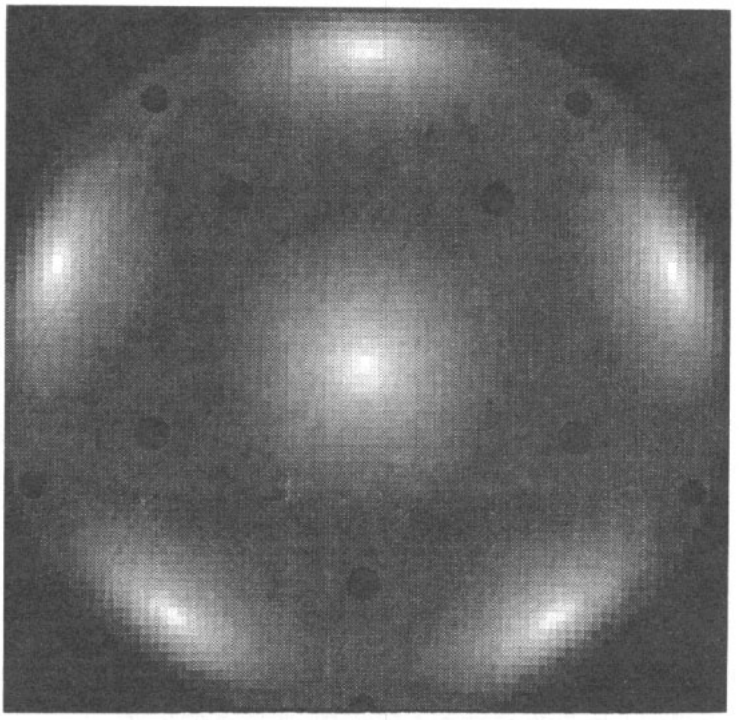

Figure 4. A density plot of the lowest APES for the G⊗h interaction projected onto spherical geometry. Dark areas indicate lower energy, black discs mark minima. Peaks in the energy, which appear white, are also degeneracies and occur at points of fivefold symmetry.

This geometry simplifies greatly the phase tracking because immediately we have the proximity of minima to neighbouring minima in terms of an easily visualized structure. For the type (II) saddle points we find $\cos 3\alpha = \sqrt{27/32}$, and although they do not lie on the same α-surface as the minima, a calculation of the distances between type (II) extrema shows that these saddle points may be considered as occupying the centres of the edges of the dodecahedron. The centres of the faces of the dodecahedron in the $\alpha = 0$

surface are twofold degeneracies on the LAPES. Tracking the phase numerically along paths between neighbouring minima via the saddle points between them we find that there are sign changes in the eigenstate corresponding to two specific types of path. First, a circuit around a pentagonal face of the dodecahedral surface in (Q, θ, ϕ)-space results in a path enclosing a degeneracy (path I, figure 5(a)). Taking path II in figure 5(a) also induces a phase change of π in the eigenstate, although it does not enclose an obvious degeneracy. A simple relabelling of the dodecahedron, making sure that nearest-neighbour minima remain the same, shows that when viewed in figure 5(b), path II does indeed enclose a degeneracy. Similarly, paths that induce sign changes but do not seem to enclose degeneracies in figure 5(b) are seen to enclose degeneracies in figure 5(a).

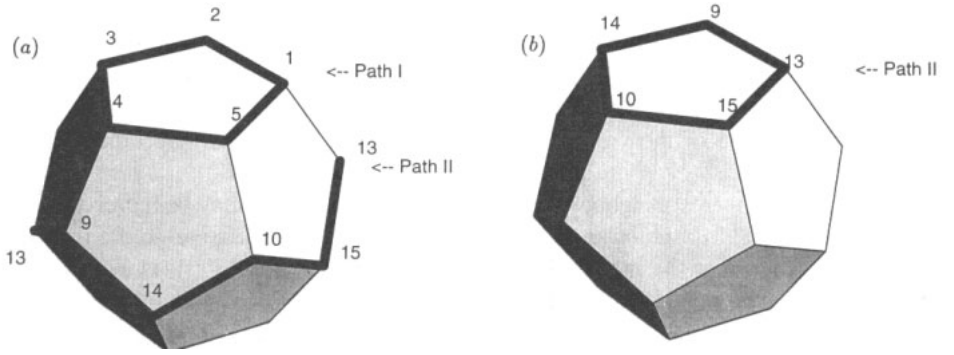

Figure 5. Mapping of the G⊗h minima onto a dodecahedron. (a) The two paths shown both induce Berry phase changes of π on the eigenstate. (b) Path II shown enclosing a degeneracy after the relabelling of the dodecahedral vertices.

It is therefore necessary to view any circuit on the lowest APES in terms of the two dodecahedra in order to see whether or not a degeneracy has been enclosed. One must not forget that the minima lie on the vertices of a dodecahedron embedded in a four-dimensional surface; and the need to map the problem on the vertices of two separate dodecahedra arises from this. We find once again that the phase properties of the eigenstates may be correctly reproduced if we implement the rule introduced in (A) for transporting eigenstates around adiabatic loops on the G⊗h LAPES.

(C) H⊗g. The ten equivalent minima in H⊗g correspond to D_{3h} distortions of the icosahedron. The coordinates of these points in phase space are just the rows of the matrix $||Q^{Hg}||$ in appendix B. Other special points on the lowest APES are as follows: A set of points of D_{3h} symmetry that are not minima are degeneracies. Points in phase space corresponding to T_h distortions are either twofold or threefold degenerate. The threefold degeneracies have lines of degeneracy running between them, and passing through those points of trigonal symmetry that are not minima. Thus the lines of degeneracy make a pattern in (a, b, α, β)-space that is not unlike that of the lines of degeneracy in G⊗g. These properties have also been established by means of various numerical scans. Phase tracking for H⊗g is slightly more complicated. We track the phase only on the paths between adjacent minima. It turns out that when the distances in phase space are calculated, each of the minima on the LAPES of H⊗g has six others as equally near neighbours. The phases are traced along closed paths going via neighbouring minima. We find that wherever such paths traverse an odd number of minima there is a Berry phase change of π, whereas an even number of minima gives no phase change. This is consistent with the rule in (A) which we also apply to this system to take proper account the Berry phase of the transported eigenstate.

5.4.2. The tunnel splitting of vibronic ground states in G⊗g, G⊗h and H⊗g at strong coupling. In the following we use a WKB approximation that allows a small amount of tunnelling between minima and nearest-neighbour minima only. The Jahn–Teller system is now *dynamical*, and the lowest states, as given by this WKB approximation, will be linear combinations of wave functions corresponding to ground-state harmonic oscillators (GSHO) in each minimum of the LAPES. These linear combinations must be invariant under the operations of the symmetry group of the Jahn–Teller centre. This amounts to saying that a translation that takes us from one minimum to another copy of itself must leave the full vibronic wave function invariant. Therefore, wherever this translation changes the sign of the electronic basis, the change of sign must be compensated for by a corresponding change of sign in the vibrational wave function so that the full vibronic wave function is unchanged. The GSHOs in the minima must therefore obey a similar rule to that imposed on the electronic eigenstates on transportation from minimum to minimum (see (A) of 5.4.1). Let the GSHO in the ith minimum be Φ_i so that its antipodal equivalent be $-\Phi_i$. The full vibronic wave function in the ith minimum is then $\Phi_i|m_i\rangle$ which equals $-\Phi_i|\bar{m}_i\rangle$. This is the required invariance of the vibronic state under a translation from one minimum to another copy of itself.

The distribution of nearest-neighbour minima for a system $\Gamma\otimes\Lambda$, may be represented in the form of a matrix $||S^{\Gamma\Lambda}||$, the bases of which are the kets that correspond to the minima in v space listed as rows of the matrix $||Q^{\Gamma\Lambda}||$ (see equation (36)). $||S^{\Gamma\Lambda}||$ is a matrix of overlaps between nearest-neighbour minima on the LAPES of $\Gamma\otimes\Lambda$. The elements $||S^{\Gamma\Lambda}_{ij}||$, of $||S^{\Gamma\Lambda}||$, are $-S$ if minimum i and minimum j are nearest-neighbour minima and zero if minimum i and j are not. The negative value of the overlap is a consequence of the sign change of the GSHOs as one translates from minimum to minimum. As an example, let us consider the corresponding overlap matrix for $G\otimes g$. In this case each minimum has four nearest neighbours so the resulting overlap matrix $||S^{Gg}||$ will be

	min 1	min 2	min 3	min 4	min 5
min 1	0	$-S$	$-S$	$-S$	$-S$
min 2	$-S$	0	$-S$	$-S$	$-S$
min 3	$-S$	$-S$	0	$-S$	$-S$
min 4	$-S$	$-S$	$-S$	0	$-S$
min 5	$-S$	$-S$	$-S$	$-S$	0

(42)

The transformation that diagonalizes $||S^{Gg}||$ is then just $\mathbf{T}(T_h)$ (defined in 5.3) which reduces the space of T_h minima in $G\otimes g$ to the irreducible spaces A and G of the icosahedral group. The diagonalization yields a G quartet state corresponding to an overlap of $+S$ and an A singlet corresponding to an overlap of $-4S$. Following a similar argument to that in [25], the positive overlap of the quartet state implies that it has a lower energy than that of the singlet of overlap $-4S$. We deduce that the energies of these ground states at strong coupling are

$$E_A = (H_{11} - 4H_{12})/(1 - 4S)$$
$$E_G = (H_{11} + H_{12})/(1 + S) \tag{43}$$

where H_{11} is the expectation value of the Hamiltonian, H, in the GSHO at any one of the minima, and H_{12} is a matrix element of H between two GSHOs in nearest-neighbour minima. The linear combinations of the GSHOs that correspond to the two overlap eigenvalues are then given by the columns of the matrix $\mathbf{T}(T_h)$.

The corresponding calculation for $G\otimes h$ and $H\otimes g$ involves the two matrices $||S^{Gh}||$ and $||S^{Hg}||$ respectively. These two matrices are constructed in the same way as $||S^{Gg}||$. The

10×10 matrix $||S^{Gh}||$ has three off-diagonal non-zero elements in each row corresponding to an overlap of $-S$ between nearest-neighbour minima in that case. The 10×10 matrix $||S^{Hg}||$ has the other six off-diagonal elements in each row non-zero, corresponding to an overlap of $-S$ between nearest-neighbour minima. The transformation that diagonalizes $||S^{Gh}||$ and $||S^{Hg}||$ is then just $\mathbf{T}(D_{3h})$ (defined in 5.3) which reduces the space of D_{3h} minima in both $G\otimes h$ and $H\otimes g$ to the irreducible spaces A, G and H of the icosahedral group. For $G\otimes h$, the diagonalization yields a G quartet, an H quintet and an A singlet of states corresponding to the overlap eigenvalues $2S$, $-S$ and $-3S$ respectively. By the same argument as before [25] we deduce that in $G\otimes h$ the lowest-lying state is the G quartet and that the energies of the ground states at strong coupling are

$$\begin{aligned} E_A &= (H_{11} - 3H_{12})/(1 - 3S) \\ E_H &= (H_{11} - H_{12})/(1 - S) \\ E_G &= (H_{11} + 2H_{12})/(1 + 2S). \end{aligned} \tag{44}$$

For $H\otimes g$, the diagonalization yields an H quintet, a G quartet and an A singlet of states corresponding to the overlap eigenvalues $2S$, $-S$ and $-6S$ respectively. By the same argument as before [25] we deduce that in $H\otimes g$ the lowest-lying state is the H quintet and that the energies of the ground states at strong coupling are

$$\begin{aligned} E_A &= (H_{11} - 6H_{12})/(1 - 6S) \\ E_G &= (H_{11} - H_{12})/(1 - S) \\ E_H &= (H_{11} + 2H_{12})/(1 + 2S). \end{aligned} \tag{45}$$

In both $G\otimes h$ and $H\otimes g$, the linear combinations of GSHOs corresponding to the overlap eigenvalues are just the columns of the matrix $\mathbf{T}(D_{3h})$.

5.4.3. Ham factors in the lowest vibronic ground states of G⊗g, G⊗h and H⊗g at strong coupling. The definition of a Ham factor is given in equation (29). Once again, let us begin by considering $G\otimes g$. In this case we identify the operator V^g with the set of operators (34) for which we already know the matrices given by the matrix $||M^G(g)||$. As only one component is needed, we choose the component of $||M^G(g)||$ with $qg_1 = 1$ and $qg_{t=2,3,4} = 0$, as our $||V^g||$. In strong coupling the vibronic states are so well localized on the LAPES that it is only necessary to find the expectation value of $||V^g||$ at each T_h minimum in order to find its matrix elements within the vibronic ground state. At a T_h minimum, m, let the electronic eigenstate be $|m\rangle$. In the basis of T_h minima listed in table 1, the electronic expectation of $||V^g||$ in the T_h minima may be represented as a diagonal matrix $||X||$ with elements $X_{mn} = \langle m|V^g|n\rangle\delta_{mn}$, which are also the elements in the first column of $||Q^{Gg}||$. For the expectation of $||V^g||$ within the full vibronic ground states at strong coupling, we now require the expectation of $||X||$ within the vibrational ground state. From 5.4.2, in the basis of the T_h minima listed in table 1, the vibrational ground state is a G quartet and is given by four of the columns of the transformation $\mathbf{T}(T_h)$. These four columns form the column-normalized matrix $||Q^{Gg}||$. The matrix of V^g in the vibronic ground state of $G\otimes g$ at strong coupling is then

$$\frac{4}{45}\,||Q^{Gg}||^T||X||||Q^{Gg}|| = \frac{3}{4}||V^g|| \tag{46}$$

where the fraction 4/45 is there because of the column-normalization. Consequently we have the result $K(G) = \frac{3}{4}$. The two Ham factors of the antisymmetric operators, T_1 and T_2, are necessarily zero.

Let us now consider a general icosahedral system $\Gamma \otimes \Lambda$. Let the icosahedral subgroup at the stable minima be $\mathcal{G}$. For $\Gamma \otimes \Lambda$ we may again simplify greatly the matrix algebra if we only consider one element of the Jahn–Teller matrix operator within the vibronic ground state. If $\mathbf{T}$ transforms the static representation of $\Gamma \otimes \Lambda$ minima into icosahedral irreps, and $\{a_\alpha(m)\}$, $\alpha = 1, 2, 3, 4$ are the components of the electronic eigenstate in the mth minimum then

$$K(\Lambda)\langle \Lambda\lambda, \Gamma i|\Gamma j\rangle = \sum_m T_{mi}T_{mj} \sum_{\alpha\beta} a_\alpha(m)a_\beta(m)\langle \Lambda\lambda, \Gamma\alpha|\Gamma\beta\rangle \tag{47}$$

is the (i, j)th element of a Λ matrix operator in the Γ vibronic ground state. The index m runs through the $\Gamma \otimes \Lambda$ minima, and the index λ runs through the components of the irrep Λ. By using the orthonormality relations of the Clebsch–Gordan coefficients, which is

$$\sum_{i,j} \langle \Lambda\lambda\Gamma i|\Gamma j\rangle\langle \Lambda\lambda'\Gamma i|\Gamma j\rangle = \delta_{\lambda,\lambda'} \tag{48}$$

and by making the observation that

$$T_{mi} = \sqrt{\frac{|\Gamma|}{N}}\, a_i(m) \tag{49}$$

where $|\Gamma|$ is the dimension of the irrep Γ and N is the number of minima, we obtain

$$K(\Lambda) = \frac{|\Gamma|}{|\Lambda|}\, \mathcal{I}(\mathcal{G}) \tag{50}$$

where $\mathcal{I}(\mathcal{G})$ is the following fourth-order invariant of the icosahedral group:

$$\mathcal{I}(\mathcal{G}) = \sum_\lambda \sum_{ij\alpha\beta} a_i(m)a_j(m)a_\alpha(m)a_\beta(m)\langle \Lambda\lambda, \Gamma i|\Gamma j\rangle\langle \Lambda\lambda, \Gamma\alpha|\Gamma\beta\rangle \qquad \forall m. \tag{51}$$

It should be noted that to get the matrix elements $\langle \Lambda\lambda, \Gamma\alpha|\Gamma\beta\rangle$ from appendix A, normalization requires an extra factor of $1/\sqrt{12}$ for $\Gamma = \mathrm{G}$ and $1/\sqrt{60}$ for $\Gamma = \mathrm{H}$. Using the relation above we calculate the Ham factors for different Λ operators at strong coupling for all the systems treated in this paper. We tabulate the results below. The two Ham factors of the antisymmetric operators, $K(\mathrm{T_1})$ and $K(\mathrm{T_2})$, within the above vibronic ground states are necessarily zero. Due to the multiplicity of H in the symmetric product H⊗H, there are two different Ham factors for the case $\Lambda = \mathrm{H}$ which must be carefully defined. For this reason we have put queries in table 2 and defer a discussion of these Ham factors to a later paper. Equation (50) is valid also for the equal-coupling case $\mathrm{G}\otimes(g \oplus h)_{\mathrm{eq}}$. In this case we may write a similar expression to equation (47) but now the sum over minima (m) will be an integral over the hyperspherical trough. The resulting fourth-order invariant is the SO(4) invariant $\mathcal{I}(\mathrm{SO}(4))$. The value of the invariant is 3/4 and multiplying this with the scaling factor 4/9 recovers the Ham factor obtained in 4.2.1 of 1/3. The Ham factor $K(\mathrm{H})$ in $\mathrm{G}\otimes g$ is zero, implying that the minima in $\mathrm{G}\otimes g$ remain minima even if the effects of h-vibrations are included. One may infer from this that the LAPES of $\mathrm{G}\otimes g$ touches the minimum-energy hypersurface of $\mathrm{G}\otimes(g \oplus h)_{\mathrm{eq}}$ at the $\mathrm{T_h}$ minima. Thus we find that on the $\mathrm{G}\otimes(g \oplus h)_{\mathrm{eq}}$ hypersurface and at the $\mathrm{T_h}$ minima, the splitting of the G state is the same. Also, the invariants $\mathcal{I}(\mathrm{T_h})$ and $\mathcal{I}(\mathrm{SO}(4))$ share a common value of 3/4. Conversely, the non-zero value of the $K(\mathrm{G})$ in $\mathrm{G}\otimes h$, implies that states corresponding to the $\mathrm{D_{3h}}$ minima may in general be further distorted to a lower energy by g-distortions.

Table 2.

	$\mathcal{I}(\mathcal{G})$, $\Lambda = \mathrm{G}$	$\mathcal{I}(\mathcal{G})$, $\Lambda = \mathrm{H}$	$K(\mathrm{G})$	$K(\mathrm{H})$
$\mathrm{G}\otimes g$	$\mathcal{I}(\mathrm{T_h}) = \frac{3}{4}$	$\mathcal{I}(\mathrm{T_h}) = 0$	$\frac{3}{4}$	0
$\mathrm{G}\otimes h$	$\mathcal{I}(\mathrm{D_{3h}}) = \frac{5}{90}$	$\mathcal{I}(\mathrm{D_{3h}}) = \frac{25}{36}$	$\frac{5}{90}$	$\frac{5}{9}$
$\mathrm{H}\otimes g$	$\mathcal{I}(\mathrm{D_{3h}}) = \frac{16}{45}$	(??)	$\frac{4}{9}$	(??)

6. The Berry phase and ground states in G⊗(g⊕h) at other relative couplings of g and h

The LAPES of G⊗(g⊕h) has two different structures depending on which of the two modes, g or h, gives rise to the larger Jahn–Teller stabilization energy. A discussion on how the LAPES of G⊗($g \oplus h$) adopts these two different structures may be found in the work of Ceulemans *et al* [9]. Here we summarize the effect of different relative couplings of the g- and h-modes on the ground states.

We should first remark that if the coupling to both sets of modes is included in the Öpik and Pryce equations (35), then the solutions are just the same as for the two modes separately, so all the solutions are as listed in table 1. We can accordingly plot all the turning point energies against the relative coupling strength, as is done in figure 6.

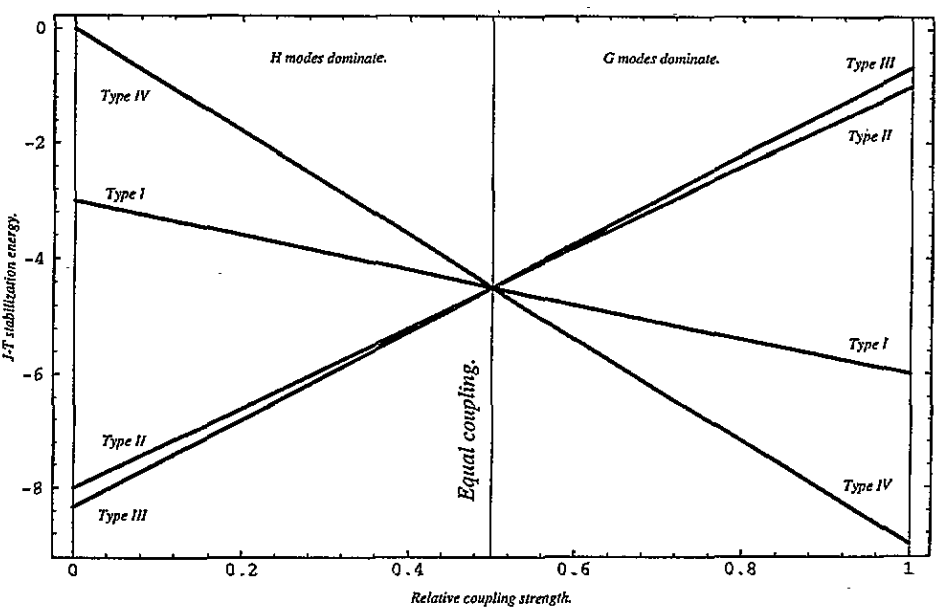

Figure 6. The energies of the Öpik and Pryce turning points in G⊗($g \oplus h$), showing how they vary with relative coupling strength.

Looking at this plot it is very obvious that only three situations arise. Whenever the g-coupling predominates the minima are of type (IV) and the path of lowest energy between them goes via the type (I) saddle points. Conversely if the h-coupling is strongest, the minima are of type (III) and the intermediate saddle points are of type (II). In the case of equal coupling all the above points coincide in energy and lie on the minimum-energy

hypersphere of $G\otimes(g\oplus h)_{eq}$ (see section 4). For brevity we shall call this hypersphere S.

To discuss the the complete structure of degeneracies and Berry phases over the full nine-dimensional phase space of $G\otimes(g\oplus h)$ would be a mammoth task. Indeed, it is a task that we did not even complete in the four- and five-dimensional phase spaces of the subsystems $G\otimes g$ and $G\otimes h$. What we did do and what is needed now is to understand how the phases change over the minimum-energy tunnelling paths between minima. We have already pointed out that at all relative coupling strengths the minima and the minimum-energy paths connecting them are either the same or closely related to those calculated for the g- and h-mode regimes separately. This means that as we move from coupling to one phonon type alone and increase the influence of the other phonon type, the topology of the minima, the tunnelling paths that connect them, the phases and the ground states will be constructed in just the same way as before.

Take for example the case when the g-mode dominates. The five minima are of type (IV), with $qh_i = 0$, $i = 1, 2, 3, 4, 5$, and the minimum-energy path available for tunnelling is via the the type (I) saddles. The difference now is that the coupling to the H modes reduces the energy of the saddles, but increases the length of the minimum-energy tunnelling paths. The path that dominates the tunnelling energy will be a compromise between these two effects, but as long as the old path can be continuously distorted into the new one without crossing a degeneracy on the LAPES, the phase relationships will be preserved. As one approaches $G\otimes(g\oplus h)_{eq}$, the coordinates of the type (IV) T_h minima on S remain as given in table 1. All these points lie on S at a θ-value of $\pi/4$, forming a lattice of these points and their antipodal equivalents on the (α, β)-surface. We find that the phase relationships between these points (and their antipodal equivalents) are consistent with the phase changes of the $G\otimes(g\oplus h)_{eq}$ eigenstate (equation (14)), so we carry the argument for identifying the vibronic ground states through from $G\otimes g$ coupling, to equal $G\otimes(g\oplus h)_{eq}$ coupling.

In a similar vein we can consider what happens as one approaches $G\otimes(g\oplus h)_{eq}$ from $G\otimes h$. The f-space coordinates of the $G\otimes h$ minima are given in table 1. In this case we do not have the simplicity of $G\otimes g$ where the minima remain minima even as we approach the equal-coupling case. In this case we check that as we increase the strength of g distortions on the $G\otimes h$ subsystem, the points corresponding to D_{3h} symmetry remain mutually equidistant. As we approach $G\otimes(g\oplus h)_{eq}$ but with the h-mode still dominant, the tunnelling between the D_{3h} points is still via the type (II) saddles. The coupling to the g-modes reduces the energy of these saddles, but increases the length of the minimum-energy tunnelling paths. The form of the overlap matrix between the D_{3h} points remains unchanged until we reach the equal-coupling regime, so we carry the argument for identifying the vibronic ground states through from $G\otimes h$ coupling, to equal $G\otimes(g\oplus h)_{eq}$ coupling.

Using these arguments we can be reasonably sure that we know the nature of the ground state at strong coupling through the various changes in relative coupling strength. We can also assume, by analogy with the similar, but simpler, cubic Jahn–Teller system $T\otimes(\epsilon\oplus\tau)$, that the Ham factors vary smoothly between the extreme values shown in table 2 via the equal-coupling value of 1/3.

7. Discussion and future work

The strong-coupling regime of the three single-mode systems ($G\otimes g$, $G\otimes h$ and $H\otimes g$) discussed here have a lot in common with each other, as well as with the system $T\otimes\tau$ in the cubic group [15]. They all have the lowest APES with a number of minima, always corresponding to symmetric distortions of the icosahedron. The number of minima is larger than the degeneracy of the initial electronic state. As a result they all have groups of low-

lying states at strong coupling that are split in energy by tunnelling matrix elements, and in each case the Berry phase changes across the surface have to be tracked, so that the ordering in energy of these states can be given correctly, and in each case the lowest state belongs to the same representation as the initial electronic state. This similarity with $T\otimes\tau$ suggests that the optical absorption band shapes for $G\otimes g$, $G\otimes h$ and $H\otimes g$ should also be rather involved, and we should have a look at those soon. Correspondingly, $G\otimes(g\oplus h)$ is comparable to the $T\otimes(\tau\oplus\epsilon)$ in cubic symmetry [28]. $T\otimes(\tau\oplus\epsilon)$ also exhibits a continuous symmetry at equal coupling of the τ- and ϵ-modes with preferential structures for the LAPES depending on which of the two modes provides the largest Jahn–Teller stabilization.

The Ham factors at strong coupling discussed in this paper are all proportional to invariants of the icosahedral sub-groups resulting from the Jahn–Teller-active modes. One ought to be able to arrive at this result via a more direct group theoretic approach which we hope to develop in a later paper.

The whole of the work in this paper has been on the strong-coupling regime, while in C_{60} in particular the Jahn–Teller coupling is probably rather weak. However, previous experience shows that many properties such as the Ham factors can be estimated by interpolating between weak coupling, treated by second-order perturbation, and the sort of results we have here. The very high degeneracies here will make a numerical approach to the properties at intermediate coupling strengths rather difficult, but again as in $T\otimes(\tau\oplus\epsilon)$, we may be able to exploit the high symmetry in the equal-coupling case to reduce the size of the matrices needed for the numerical work.

As is clear from a comparison of the introduction with the contents of this paper, there is still any amount of work waiting to be done on this fascinating set of problems.

Appendix A. The JT interaction matrices for $G\otimes(g\oplus h)_{eq}$, $G\otimes g$ and $G\otimes h$

The matrices are, for $||M^G([g\oplus h]_{eq})||$:

$$k^G_{eq}\sqrt{3}\begin{pmatrix} q_1-\sqrt{2}q_6 & \sqrt{2}q_7 & -q_2+q_4 & q_3+q_5 \\ \sqrt{2}q_7 & -q_1+\sqrt{2}q_6 & q_3-q_5 & q_2+q4 \\ -q_2+q_4 & q_3-q_5 & q_1-\sqrt{2}q_8 & \sqrt{2}q_9 \\ q_3+q_5 & q_2+q_4 & \sqrt{2}q_9 & q_1+\sqrt{2}q_8 \end{pmatrix} \tag{A1}$$

for $||M^G(g)||$:

$$k^G_g\sqrt{2}\begin{pmatrix} -qg_3 & -qg_4 & -qg_1+qg_3 & -qg_2-qg_4 \\ -qg_4 & qg_3 & qg_2-qg_4 & -qg_1-qg_3 \\ -qg_1+qg_3 & qg_2-qg_4 & qg_1 & -qg_2 \\ -qg_2-qg_4 & -qg_1-qg_3 & -qg_2 & -qg_1 \end{pmatrix} \tag{A2}$$

for $||M^G(h)||$:

$$k^G_h\begin{pmatrix} 2qh_2-\sqrt{3}qh_1 & 2qh_5 & qh_2-qh_4 & qh_3-qh_5 \\ 2qh_5 & -\sqrt{3}qh_1-2qh_2 & -qh_3-qh_5 & -qh_2-qh_4 \\ qh_2-qh_4 & -qh_3-qh_5 & \sqrt{3}qh_1-2qh_4 & -2qh_3 \\ qh_3-qh_5 & -qh_2-qh_4 & -2qh_3 & \sqrt{3}qh_1+2qh_4 \end{pmatrix} \tag{A3}$$

and, for $||M^{H}(g)||$:

$$k_g^H \begin{pmatrix} 0 & 2\sqrt{3}qg_4 & -2\sqrt{3}qg_1 & 2\sqrt{3}qg_3 & -2\sqrt{3}qg_2 \\ 2\sqrt{3}qg_4 & 4qg_3 & -qg_1+qg_2 & -qg_3-qg_4 & -4qg_1 \\ -2\sqrt{3}qg_1 & -qg_1+qg_2 & -4qg_4 & 4qg_2 & qg_3-qg_4 \\ 2\sqrt{3}qg_3 & -qg_3-qg_4 & 4qg_2 & 4qg_4 & -qg_1-qg_2 \\ -2\sqrt{3}qg_2 & -4qg_1 & qg_3-qg_4 & -qg_1-qg_2 & -4qg_3 \end{pmatrix}. \tag{A4}$$

Appendix B. The matrices $||Q^{Gg}||$, $||Q^{Gh}||$ and $||Q^{Hg}||$

The matrix for $||Q^{Gg}||$, in units of k_g^G/ω_g^2, is

	qg_1	qg_2	qg_3	qg_4
min 1	$-3/\sqrt{2}$	0	$3/\sqrt{2}$	0
min 2	$p3$	$-p1$	$-p4$	$-p2$
min 3	$p3$	$p1$	$-p4$	$p2$
min 4	$-p4$	$-p2$	$p3$	$p1$
min 5	$-p4$	$p2$	$p3$	$-p1$

where $\left\{ \begin{array}{l} p_1 = \frac{3}{\sqrt{2}}\cos(3\pi/10) \\ p_2 = \frac{3}{\sqrt{2}}\cos(\pi/10) \\ p_3 = \frac{3}{\sqrt{2}}\sin(3\pi/10) \\ p_4 = \frac{3}{\sqrt{2}}\sin(\pi/10) \end{array} \right\}$ (B1)

(in this matrix: row-norm = $\sqrt{9}$, column-norm = $\sqrt{45/4}$). The matrix for $||Q^{Gh}||$, in units of k_h^G/ω_h^2 is

	qh_1	qh_2	qh_3	qh_4	qh_5
min 1	μ_1	μ_2	μ_3	μ_4	μ_5
min 2	μ_1	$-\mu_6$	$-\mu_7$	$-\mu_6$	μ_8
min 3	μ_1	$-\mu_9$	0	μ_{10}	0
min 4	μ_1	$-\mu_6$	μ_7	$-\mu_6$	$-\mu_8$
min 5	μ_1	μ_2	$-\mu_3$	μ_4	$-\mu_5$
min 6	$-\mu_1$	μ_6	μ_8	μ_6	μ_7
min 7	$-\mu_1$	$-\mu_4$	$-\mu_5$	$-\mu_2$	μ_3
min 8	$-\mu_1$	$-\mu_{10}$	0	μ_9	0
min 9	$-\mu_1$	$-\mu_4$	μ_5	$-\mu_2$	$-\mu_3$
min 10	$-\mu_1$	μ_6	$-\mu_8$	μ_6	$-\mu_7$

where $\left\{ \begin{array}{l} \mu_1 = \sqrt{\frac{5}{3}} \\ \mu_2 = \frac{\sqrt{5}}{3}x^{-4} \\ \mu_3 = \frac{5}{3}x \\ \mu_4 = \frac{\sqrt{5}}{3}x^4 \\ \mu_5 = \frac{5}{3}x^{-1} \\ \mu_6 = \frac{\sqrt{5}}{3} \\ \mu_7 = \frac{5}{3}x^3 \\ \mu_8 = \frac{5}{3}x^{-3} \\ \mu_9 = \frac{2\sqrt{5}}{3}x^{-2} \\ \mu_{10} = \frac{2\sqrt{5}}{3}x^2 \end{array} \right\}$ (B2)

where $x = \sqrt{(\sqrt{5}-1)/2}$ and also $x^2 = \cos(2\pi/5)$ (in this matrix: row-norm = $\sqrt{25/3}$, column-norm = $\sqrt{50/3}$). The matrix for $||Q^{Hg}||$, in units of k_g^H/ω_g^2 is

	qg_1	qg_2	qg_3	qg_4
min 1	$a\sin 0.1\pi$	$-a\cos 0.1\pi$	$-b\sin 0.3\pi$	$-b\cos 0.3\pi$
min 2	$-a\sin 0.7\pi$	$-a\cos 0.7\pi$	$b\sin 0.1\pi$	$-b\cos 0.1\pi$
min 3	$a\sin 0.5\pi$	0	$b\sin 0.5\pi$	0
min 4	$-a\sin 0.3\pi$	$-a\cos 0.3\pi$	$b\sin 0.9\pi$	$-b\cos 0.9\pi$
min 5	$a\sin 0.9\pi$	$-a\cos 0.9\pi$	$-b\sin 0.7\pi$	$-b\cos 0.7\pi$
min 6	$-b\sin 0.9\pi$	$-b\cos 0.9\pi$	$a\sin 0.7\pi$	$-a\cos 0.7\pi$
min 7	$b\sin 0.3\pi$	$-b\cos 0.3\pi$	$-a\sin 0.9\pi$	$-a\cos 0.9\pi$
min 8	$-b\sin 0.5\pi$	0	$-a\sin 0.5\pi$	0
min 9	$b\sin 0.7\pi$	$-b\cos 0.7\pi$	$-a\sin 0.1\pi$	$-a\cos 0.1\pi$
min 10	$-b\sin 0.1\pi$	$-b\cos 0.1\pi$	$a\sin 0.3\pi$	$-a\cos 0.3\pi$

(B3)

with $a = (8/3)((\sqrt{5}-1)/2)^{-1}$ and $b = (8/3)(\sqrt{5}-1)/2$ (in this matrix: row-norm = $\sqrt{64/3}$, column-norm = $\sqrt{160/3}$).

References

[1] Kroto H W, Heath J R, O'Brien S C, Curl R F and Smalley R E 1985 *Nature* **318** 162–3
[2] Judd B R 1957 *Proc. R. Soc.* A **241** 122–31
[3] Pooler D R 1980 *J. Phys. C: Solid State Phys.* **13** 1029–42
[4] Negri F, Orlandi G and Zerbetto F 1988 *Chem. Phys. Lett.* **144** 31–7
[5] Lannoo M, Baraff G A, Schlüter M and Tomanek D 1991 *Phys. Rev.* B **44** 12 106–8
[6] de Coulon V, Martins J L and Reuse F 1992 *Phys. Rev.* B **45** 13 671–5
[7] Auerbach A and Manini N 1994 *Phys Rev* B **49** 12 998–3007
[8] Auerbach A and Manini N 1994 *Phys Rev* B **49** 13 008–16
[9] Ceulemans A and Fowler P W 1989 *Phys. Rev.* A **39** 481–93
[10] Ceulemans A and Fowler P W 1990 *J. Chem. Phys.* **93** 1221–34
[11] Khlopin V P, Polinger V Z and Bersuker I B 1978 *Theor. Chim. Acta (Berlin)* **48** 87–101
[12] O'Brien M C M 1971 *J. Phys. C: Solid State Phys.* **4** 2045–63
[13] Fletcher J R, O'Brien M C M and Evangelou S N 1980 *J. Phys. A: Math. Gen.* **13** 2035–47
[14] Murray-Rust P, Buergi H B and Dunitz J D 1979 *Acta Crystallogr.* A **35** 703
[15] Ceulemans A, Beyens D and Vanquickenbourne L G 1984 *J. Am. Chem. Soc.* **106** 5824–37
[16] Barut A O and Raczka R 1986 *Theory of Group Representations and Applications* (Singapore: World Scientific) pp 302–7
[17] Berry M V 1984 *Proc. R. Soc.* A **392** 45–57
[18] Aitchison I J R 1988 *Phys. Scr.* T **23** 12–20
[19] Ham F S 1987 *Phys. Rev. Lett.* **58** 725–8
[20] Ham F S 1965 *Phys. Rev.* A **138** 1727–39
[21] Ham F S 1968 *Phys. Rev.* **166** 307–21
[22] Biedenharn L C 1961 *J. Math. Phys.* **2** 433–41
[23] Ceulemans A 1987 *J. Chem. Phys.* **87** 5374–85
[24] Öpik U and Pryce M H L 1957 *Proc. R. Soc.* A **238** 425–47
[25] O'Brien M C M 1989 *J. Phys. A: Math. Gen.* **22** 1779–97
[26] O'Brien M C M 1971 *J. Phys. C: Solid State Phys.* **4** 2524–36
[27] Golding R M 1973 *Mol. Phys.* **26** 661–672
[28] O'Brien M C M 1969 *Phys. Rev.* **187** 407–18